![CHALMERS UNIVERSITY OF TECHNOLOGY]

Sidelobe blanking in the presence of noise-like interference

Master's thesis in Applied Physics

Stina Wahlgren

MASTER'S THESIS 2018

Sidelobe blanking in the presence of noise-like interference

STINA WAHLGREN *

Department of Space, Earth and Environment
Division of Microwave and Optical Remote Sensing
CHALMERS UNIVERSITY OF TECHNOLOGY
Gothenburg, Sweden 2018

*Contact: wahlgrenstina@gmail.com

Sidelobe blanking in the presence of noise-like interference
STINA WAHLGREN

Supervisor: Björn Hallberg, Saab Surveillance
Supervisor: Erik Blomberg, Department of Space, Earth and Environment
Examiner: Lars Ulander, Department of Space, Earth and Environment

Abstract

Interference suppression in antenna arrays is an important topic for target detection in radar systems. This thesis investigates the performance of two different algorithms for determining whether a detection lies in the sidelobe or mainlobe of an antenna in the presence of noise-like interference (NLI). Both algorithms are based on a combination of sidelobe blanking (SLB) and sidelobe cancellation (SLC). The first algorithm is a simple cascading of SLC and SLB, while the second algorithm is a modification of this where multiple guard channels are used. The performance is evaluated with Monte Carlo simulations, where the antenna is modelled as a linear phased-array antenna and interference and target signals are modelled as uncorrelated, single-frequency plane waves. The influence of covariance estimation error, number of NLI sources, placement of auxiliary antennas, signal-to-noise ratio (SNR) and jammer-to-noise ratio (JNR) on performance and suitable blanking threshold is investigated. It is shown that the second algorithm performs better than the first when the number of NLI sources are few relative to the number of auxiliary antennas, and reduces to the same performance as the first algorithm when this is not the case.

Sidelobe blanking in the presence of noise-like interference
STINA WAHLGREN
Department of Space, Earth and Environment
Chalmers University of Technology

Sammanfattning

Störundertryckning i antenner är viktigt för att kunna detektera mål korrekt i radarsystem. I det här projektet har prestandan hos två olika algoritmer undersökts, med syfte att avgöra om en detektion kommer från en antenns huvudlob eller sidlob, då antennen belyses av störare. Båda algoritmerna bygger på en kombination av sidlobsblankning (SLB) och adaptiv sidlobsundertryckning (ASLU). Den första algoritmen är en enkel kaskadkoppling av SLB och ASLU, medan den andra algoritmen är en modifikation av den förra med multipla vaktkanaler. Prestandan har utvärderas med hjälp av Monte Carlo-simuleringar, där antennen modellerats som en linjär gruppantenn bestående av isotropa antennelement, medan stör- och målsignaler modellerats som okorrelerade, monokroma, plana vågor. Effekten av kovariansskattningsfel, antal störare, placering av hjälpantenner, signal-brusförhållande och stör-brusförhållande på prestanda och lämpliga tröskelvärden för SLB har undersökts. Den andra algoritmen presterar bättre än den första då antalet störare är få relativt antalet hjälpantenner. Skillnaden i prestanda mellan algoritmerna minskar då antalet störare ökar.

Acknowledgements

Contents

Contents

x

Nomenclature

Abbreviations

ECCM   Electronic counter-countermeasures

ECM   Electronic countermeasures

JNR   Jammer-to-noise ratio

NLI   Noise-like interference

SLB   Sidelobe blanking

SLC   Sidelobe cancellation

SNR   Signal-to-noise ratio

Operators

$\overline{(\cdot)}$ Complex conjugate

$\mathrm{Cov}[\,\cdot\,]$ Covariance

$(\cdot)^{\mathrm{H}}$ Hermitian transpose

$(\cdot)^{\mathrm{T}}$ Transpose

$\mathrm{E}[\,\cdot\,]$ Expected value

$\mathrm{diag}(\mathbf{v})$ Diagonal matrix with diagonal entries $\mathbf{v}$

Variables

θ Angle of incidence

J Number of NLI-jammers

M Number of auxiliary antennas

N Number of antenna elements

u Sinus of angle of incidence

Y Youden's index

$\varepsilon^{\mathrm{cal}}$ Calibration errors

$\mathbf{Q}$ Covariance matrix

Contents

1
Introduction

A radar system uses electromagnetic energy in the radio- or microwave range to measure range and direction to targets. The basic principle is that energy pulses are transmitted in a certain direction and the time between transmission and detection of reflected waves is used to measure the distance to the reflecting objects.

The first radar like invention, the telemobiloscope, was patented in 1904 by the German physicist Christian Hülsmeyer, but it would take until shortly before the second world war until the first effective radar systems were developed. The first radar systems were primarily a British invention, aimed as an early warning system for detecting bombers [1]. The first systems used enormous antennas, with wavelengths of around 10 metres. During the war, new inventions made it possible to use shorter wavelengths (centimetres), which opened up new military applications. Radar technology has continued to evolve. Today radars are used in a variety of fields, both military applications, such as surveillance, missile defence systems, missile launching systems, and civil applications, for instance flight radar, weather radar or radars in modern cars. Other applications, such as biomass measurements of forests [2] or breast tumour detection [3], are still at the research stage.

A highly simplified block diagram of the general principles of a modern radar system is shown in Figure 1.1. The general components of a radar system can be divided into: a transmitter, a transmitting antenna, a receiving antenna, a receiver, a signal processing unit and in general a data processing unit [4]. The purpose of the transmitter is to generate suitable waveforms that the transmitting antenna propagates in the desired direction. A receiving antenna collects the reflected energy and passes the signals to the receiver. In monostatic radars the same antenna is used for both transmission and reception. In the signal processing step, data, such as if a target was detected and if so at what range the target lies, is extracted from the received signals. The data processing step includes for example target tracking. This thesis is focused at the signal processing step, or more precisely at the task of
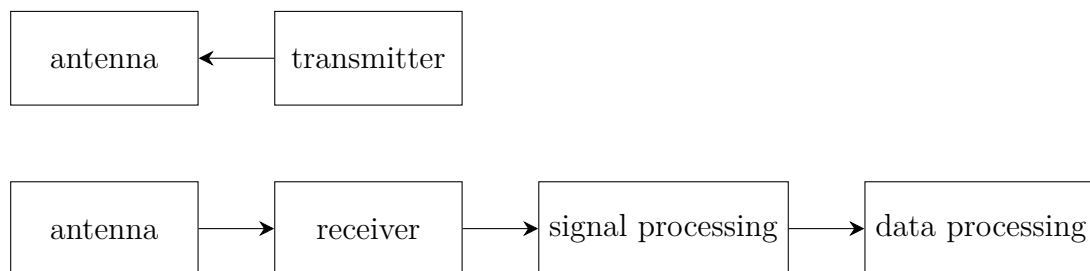

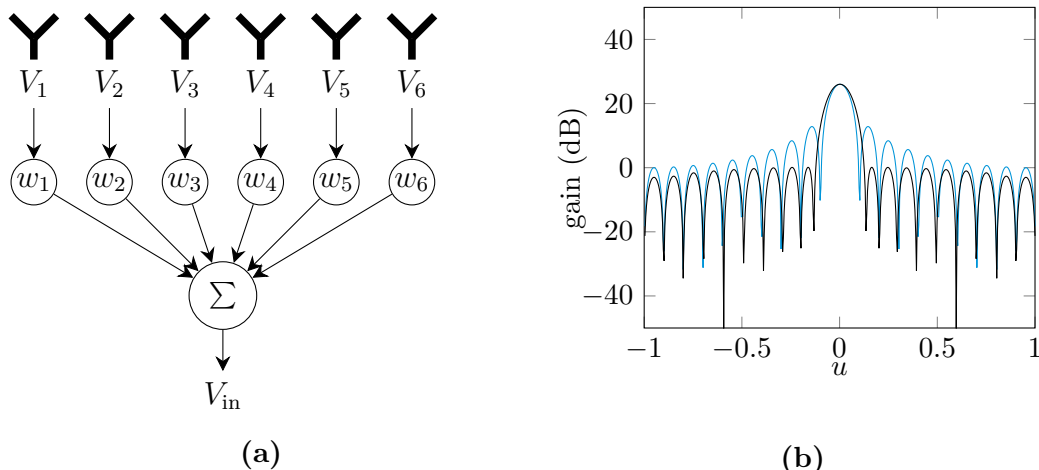**Figure 1.1:** General design of a modern radar system.

Figure 1.2: Block diagram of a uniform linear antenna array with 6 antenna elements (a) and comparison between uniform tapering (blue) and Taylor tapering (black) (b). u is sinus of the incidence angle, i.e. the angle between the plane wave and the linear array.

detection decision.

1.1 Phased-array antennas

A common antenna type used in radar technology is the phased-array antenna. It consists of many smaller antennas, called antenna elements, where the phase and amplitude of each element can be individually controlled [5]. The most common antenna elements are slots, dipoles, open-ended waveguides or patches [5]. In this project they are treated as points with an isotropic antenna pattern, that is they have the same gain in all directions.[1] The main advantage of phased-array antennas is that the beam can be steered electronically, which reduces the time it takes to change beam direction to a fraction of the time it would take to change the orientation of the antenna mechanically. This makes the antenna much more flexible [5]. Phased-array antennas come in many forms. Depending on the application, the antenna elements can be arranged in one or two dimensions, the surface flat or curved and the spacing between elements uniform or irregular. In this thesis, a one-dimensional, linear, uniform antenna array is used.

A schematic illustration of a phased-array antenna is shown in Figure 1.2a. The signals received by the antenna elements are combined to a main channel, with a higher directivity. Steering of the beam is achieved by phase shifting the signals from the antenna elements in such a way that signals from the desired direction experience constructive interference. Uniqueness is achieved by ensuring that the antenna elements are at most half a wavelength apart.

An ideal radar beam is as narrow as possible, for a high resolution in direction, and with as low sidelobe levels as possible. In order to reduce the sidelobe levels,

---

[1]Note that like spherical cows, such antennas do not exist in the real world. In contrast to spherical cows however, this simplification is in general considered useful.

tapering can be applied to phased-array antennas. Tapering is simply to change the amplitude of the signals from the antenna elements before combining them to the main channel. Tapering always comes with the cost of broadening of the mainlobe. A common tapering in radar technology is Taylor tapering, which provides a strong sidelobe suppression with a minimum broadening of the mainlobe [6]. It is defined by the following three parameters: (i) the number of antenna elements, N, (ii) the desired maximum sidelobe level, SLL, and (iii) the number of nearly constant sidelobes adjacent to the mainlobe, $\bar{n}$. Figure 1.2b shows the effect of Taylor tapering on a typical phased-array antenna pattern.

In theory, each antenna element can have its own receiver, which opens up a lot of possibilities, such as multiple simultaneous beams. Due to practical limitations, this is rarely the case in real radar systems. In general, beamforming is made before the receiver, which means that only combined channels are accessible for digital signal processing.

1.1.1   Phase shift between two antenna elements

The phase shift of an incident plane wave between two antenna elements is used later in this report, so we make a quick derivation of it here. Suppose the incoming wave has an incidence angle θ and wavelength λ, as illustrated in Figure 1.3. If the distance between the antenna elements is $\tilde{d}$, the phase shift, φ, between the signals from the two antenna elements is

$$\varphi = \frac{2\pi}{\lambda}\tilde{d}\sin(\theta)$$

If the distance between adjacent antenna elements is $\lambda/2$, the equation above simplifies to

Figure 1.3: Schematic illustration of an incident plane wave. The black dots represent two antenna elements.

$$\varphi = \pi d \sin(\theta), \tag{1.1}$$

where the integer d is the number of half wavelengths between the two antenna elements. Due to the fact that the phase shift depends on sinus of angle of incidence, it is common to introduce the variable $u = \sin\theta$.

1.2   Electronic counter-countermeasures

Electronic counter-countermeasures (ECCM) is an umbrella term for techniques developed in order to avoid or reduce the effect of electronic countermeasures (ECM). The purpose of ECM techniques is to deny the victim radar information or supply it with misleading information [7][8]. There are numerous different ECM methods, ranging from releasing a cloud of thin metal foils (chaff) in order to screen the target or otherwise confuse the radar system, to active transmission of signals. One class of ECM is the so called *jamming*, which can be defined as the intentional and deliberate transmission or retransmission of signals for the purpose of disturbing or deceiving radar systems [8].
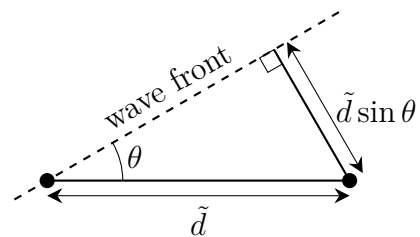
One problem that arises in radar technology is that the antenna typically has sidelobes, which means that energy arriving at the antenna from a different angle than the mainlobe direction can enter the receiver, although with a lower gain than energy entering via the mainlobe. This phenomenon is exploited in sidelobe jamming. This thesis is concerned with two types of sidelobe jamming, namely *false target jamming* and *noise-like interference* (NLI). In false target jamming the jammer transmits (or retransmits) energy pulses, which if they enter the receiver via antenna sidelobes can be misinterpreted as a weaker signal entering via the mainlobe. Thus, the effect of false target jamming is to introduce false detections. NLI on the other hand is continuous signals, which if they enter the antenna via sidelobes cause an overall increase of the noise level, i.e. decrease in SNR [9]. Thus, the effect of NLI is to make it harder to detect targets.

Two ways to handle the types of sidelobe jamming mentioned above is *sidelobe blanking* (SLB), aimed at false target jamming, and *sidelobe cancellation* (SLC), aimed at NLI [7]. Both methods belong to the class of antenna-related ECCM, that is they use additional antennas in order to reduce the effect of jamming [8]. The additional antennas are often called guard antennas, used for SLB, and auxiliary antennas, used for SLC. In the rest of the section, both methods are treated in some detail.

Although the discussion here regards deliberate interference of the radar, the same principles applies to non-malicious sidelobe interference, such as other radars, strong scatterers in sidelobe directions, or even radio frequency interference from for instance satellites or the sun, which can be a problem in radio astronomy [10].

1.2.1 Sidelobe Blanking

SLB is a well established technique in radar for cancelling (intentional or unintentional) impulsive interference, for instance false target jammers [11]. In SLB an auxiliary antenna, the guard antenna, with a more isotropic antenna pattern is used in addition to the main antenna [8]. The amplitude of the received signal from the main antenna can then be compared with the amplitude of the received signals from the guard antenna, which makes it possible to determine if the signal entered the main antenna via a sidelobe or the mainlobe. More precisely, if V_m is the signal from the main antenna and V_g is the signal from the guard antenna, the blanking logic scheme is simply

$$\begin{cases} \dfrac{|V_m|}{|V_g|} & \geq T \quad \text{no blanking} \\[2em] \dfrac{|V_m|}{|V_g|} & < T \quad \text{blanking,} \end{cases} \tag{1.2}$$

where T is the blanking threshold. An illustration of schematic antenna pattern for the main- and guard antenna is shown in Figure 1.4a.

In the absence of NLI, SLB has been shown to be effective against false targets with small loss in true detections [12].
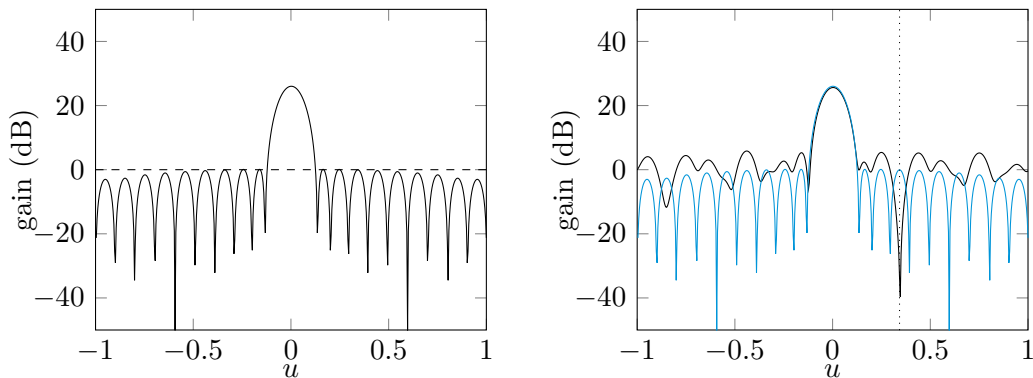
(a) Illustration of the antenna pattern of a main antenna (black) and a guard antenna (dashed) used for SLB.

(b) Illustration of the antenna pattern before (blue) and after (black) SLC introducing a null in the marked direction.

Figure 1.4: Schematic illustrations of SLB and SLC.

1.2.2 Sidelobe cancellation

The idea behind SLC is to use signals from auxiliary antennas to adaptively cancel out signals from the directions of the jammers, thus introducing nulls in the antenna pattern in those directions [7]. This will distort the antenna pattern in other directions as well, but the distortion of the mainlobe is in general negligible assuming the gain of the sidelobes is low. An illustration of the effect of SLC in an antenna pattern is shown in Figure 1.4b.

The challenge of SLC is to find the complex weights to the signals from the auxiliary antennas so that jammer signal is nullified. This is accomplished by finding the weights that minimise the output power, P_m, of the main channel when no target signal is present [13].

$$P_m = \mathrm{E}\left[V_m \overline{V_m}\right],$$

where V_m is the signal of the main channel after SLC. V_m is given by

$$V_m = V_{\mathrm{in}} - \mathbf{w} \cdot \mathbf{V}_a,$$

where V_{in} is the signal from the main antenna, $\mathbf{w}$ is the weights and $\mathbf{V}_a$ is the signals from the auxiliary antennas. Under the assumption that the jammer signals and target signal are statistically independent, the weights $\mathbf{w}$ that minimise P_m is the weights that will be best at cancelling out jammer signals, in the sense that they will cause the maximum SNR.

One set of weights that minimise P_m is

$$\mathbf{w} = \mathbf{Q}^{-1}\mathbf{R}, \tag{1.3}$$

where $\mathbf{Q}$ is the covariance matrix of the (noise and jammer only) signals from the auxiliary antennas, with elements

$$Q_{nm} = \mathrm{Cov}[V_{a_n}, V_{a_m}],$$

and $\mathbf{R}$ is the covariance vector, with elements

$$R_n = \text{Cov}[V_{\text{in}}, V_{a_n}].$$

For a derivation of this result, see for example [13].

1.2.2.1 On the number of possible nulls

Suppose a system with M auxiliary antennas is illuminated with NLI jammers from J different directions. The problem of finding weights $\mathbf{w}$ for the signals $\mathbf{V}_a$ that null the signal V_m in the directions $\{u_i\}$ of the jammers can be described as a system of linear equations

$$\begin{cases} V_{\text{in}}(u_1) - w_1 V_1(u_1) - w_2 V_2(u_1) - \cdots - w_M V_M(u_1) = 0 \\ V_{\text{in}}(u_2) - w_1 V_1(u_2) - w_2 V_2(u_2) - \cdots - w_M V_M(u_2) = 0 \\ \qquad\qquad\qquad\qquad \vdots \\ V_{\text{in}}(u_J) - w_1 V_1(u_J) - w_2 V_2(u_J) - \cdots - w_M V_M(u_J) = 0 \end{cases}$$

or equivalently

$$\begin{bmatrix} V_1(u_1) & \dots & V_M(u_1) \\ \vdots & \ddots & \vdots \\ V_1(u_J) & \dots & V_M(u_J) \end{bmatrix} \begin{bmatrix} w_1 \\ \vdots \\ w_M \end{bmatrix} = \begin{bmatrix} V_{\text{in}}(u_1) \\ \vdots \\ V_{\text{in}}(u_J) \end{bmatrix} \tag{1.4}$$

Call the matrix in the latter equality A. It is clear that the problem is solvable if $\text{rank}(A) \geq J$, and that if $\text{rank}(A) > J$ the weights $\mathbf{w}$ can be chosen in infinitely many ways. Note that A depends on both placement of auxiliary antennas and jammer directions.

1.2.3 SLC in guard channel

In contrast to SLC in an antenna with high directivity, SLC in a low-directivity antenna significantly distorts the antenna pattern in other directions as well. Since SLB is built on the comparison of signals from high- and low-directivity antennas, it is reasonable to expect the ability to determine whether a target is located in the mainlobe or not with SLB to change in the presence of NLI. The combination of SLC and SLB has been studied in [14], where it is shown that cascading SLC and SLB works well for the case of one jammer, one auxiliary antenna and no calibration or covariance estimation errors. However, we are not aware of any published results regarding performance of combined SLC and SLB methods for more complex scenarios.

1.3 Aim

The aim of this master's thesis is to investigate how a number of isotropic auxiliary antennas can be used to determine whether a target signal is located in the mainlobe or in a sidelobe of the main antenna, when the main antenna is illuminated by one or more NLI jammers. Such algorithms are called guard functions for the rest of this report.

1.4 Limitations

The focus of this project lies on general principles of SLB in the presence of NLI, therefore implementation details are not treated. The guard functions are evaluated using simulations. Targets and jammers are assumed to be far away from the radar, and jammers entering the mainlobe of the radar antenna are not considered. All target and jammer signals are assumed to be uncorrelated and monochromatic. Clutter is not modelled. Other signal processing than guard functions, e.g. pulse compression or doppler processing, are not modelled.

2
Methods

2.1 Tested guard functions

Three different guard functions are evaluated in this report, here called: No SLCg, SLCg and SLCg max. They all use sidelobe blanking logic presented in (1.2) and are compared to the same sum channel V_m. Block diagrams of the three algorithms are presented in Figure 2.1. The difference between the three methods is how V_g is defined. In No SLCg V_g is simply the signal from the guard antenna. In SLCg, V_g is the signal from the guard antenna after sidelobe cancellation using $\mathbf{V}_a$. SLCg max is similar to the second algorithm, but here all auxiliary antennas and the guard antennas are used one at a time as the guard antenna, and the other used as auxiliary antennas in SLC. Thus $M + 1$ potential guard channels V_{g_i} are created and V_g is chosen as the maximum of those:

$$V_g = \max_i\{V_{g_i}\}$$

The motivation behind SLCg max is to reduce anisotropy in the guard channel in non-jammer directions. Example of guard channel patterns are shown in Figure 2.2. SLCg was proposed in [14] and SLCg max is a modification of another algorithm presented in the same paper. In both SLCg and SLCg max the weights of the guard and auxiliary antennas are normalised, so that

$$\sum_{i=1}^{M+1} w_i\overline{w_i} = 1. \tag{2.1}$$

Note that when $J = M$, no more than one combination of weights that fulfils both (1.4) and (2.1), i.e. normalised weights that both places nulls in all jammer directions, can exist. This means that SLCg max and SLCg will produce the same result when $J = M$, provided that solutions to (1.4) exists for all choices of guard antennas.

2.2 Evaluation of performance

The purpose of the investigated methods is to determine whether a potential detection, i.e. a signal in the main channel significantly higher than the noise level, comes from the mainlobe or the sidelobes of the antenna. For the rest of the report potential detections stemming from signals entering the antenna via the mainlobe

V_{in} $\mathbf{V}_a$ V_{in}^g

SLC

V_m

V_g

SLB

detection

(a) No SLCg

V_{in} $\mathbf{V}_a$ V_{in}^g

SLC   SLC

V_m V_g

SLB

detection

(b) SLCg

V_{in} $\mathbf{V}_a$ V_{in}^g

SLC   SLC cycle guard

V_{g_1} $\cdots$ $V_{g_{M+1}}$

V_m max

V_g
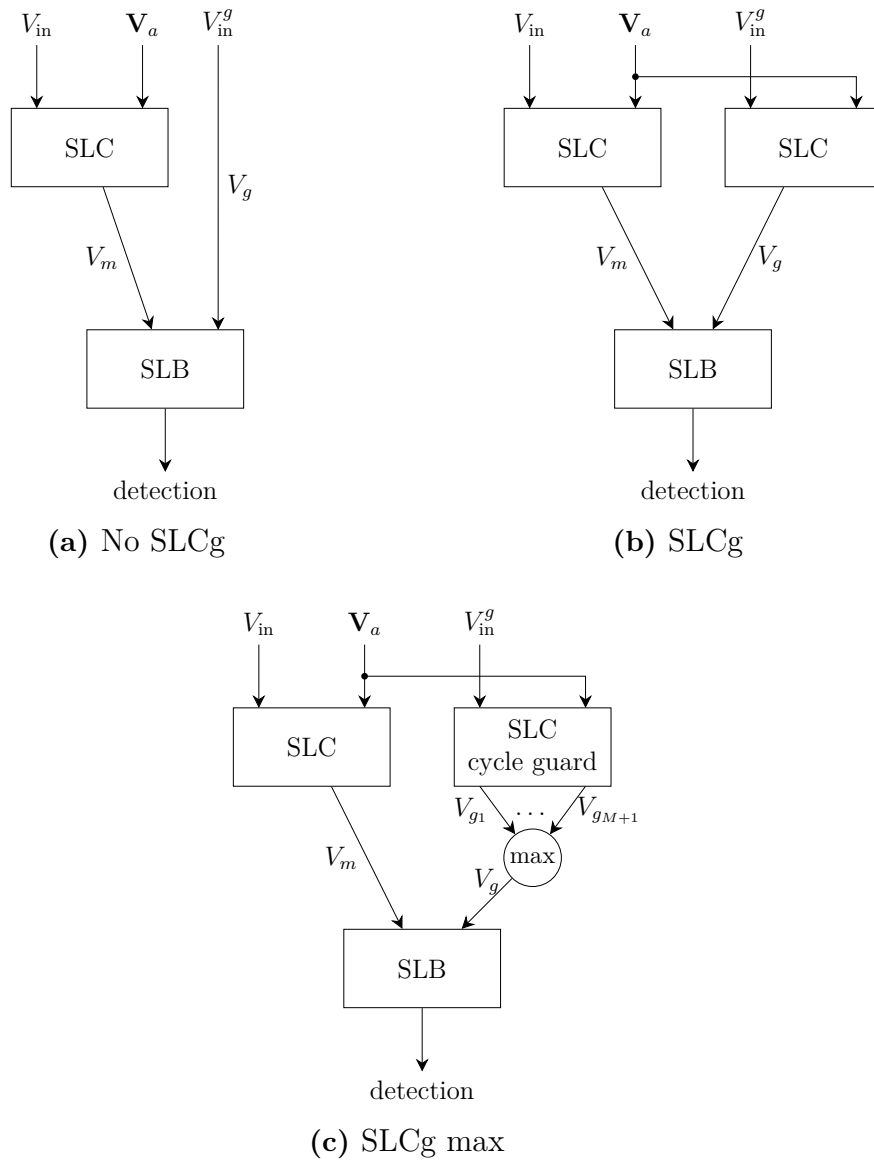
SLB

detection

(c) SLCg max

Figure 2.1: Schematic illustrations of the evaluated guard functions. V_{in} is the signal from the main antenna, $\mathbf{V}_a$ the signals from the auxiliary antennas and V_{in}^g the signal from the guard antenna.
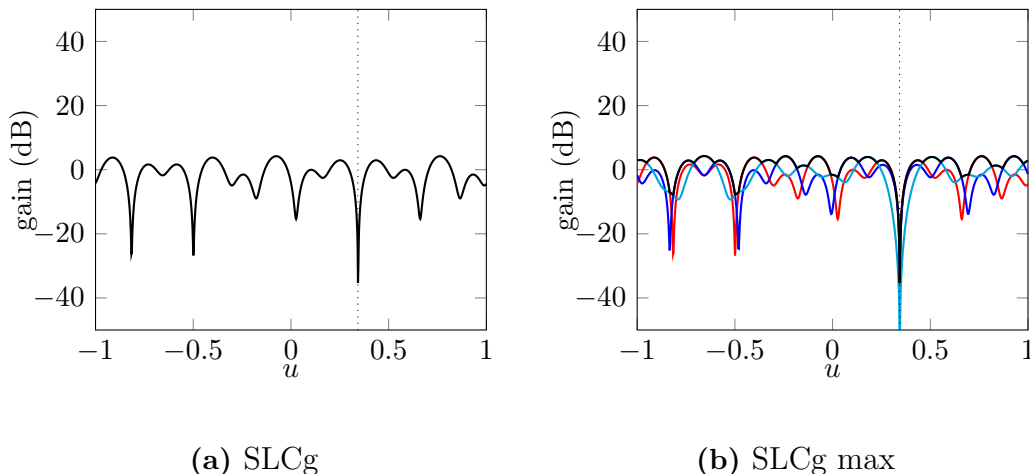
(a) SLCg

(b) SLCg max

Figure 2.2: Example of the antenna patterns of guard channels produced by SLCg and SLCg max. In b), the antenna pattern for each choice of guard channel is shown in colours and the maximum of those is marked with black.

are called *true targets* while those stemming from signals entering the antenna via sidelobes are called *false targets*.

In order to evaluate the performance of the methods, we focus on two quantities, namely the probability of detection, P_d, and the probability of false alarm, P_{fa}. P_d is defined as the probability of a true target correctly classified as a true target and P_{fa} is the probability of a false target falsely classified as a true target. Using the blanking logic in (1.2) results in the following expressions

$$P_d(T) \quad = P\left(\frac{|V_m|}{|V_g|} > T \middle| \text{true target}\right)$$

$$P_{fa}(T) \quad = P\left(\frac{|V_m|}{|V_g|} > T \middle| \text{false target}\right)$$

where T is the blanking threshold.

2.2.1   Model

The main antenna is modelled as a linear phased-array antenna with 100 antenna elements, modelled as points with isotropic antenna patterns for all polarisations. The antenna is tapered using a Taylor tapering with SLL $= -40\,\text{dB}$ and $\bar{n} = 6$. One of the antenna elements is also used as a guard antenna and three other antenna elements are also used as auxiliary antennas. Thus, in total the system consists of one main antenna and four additional antennas. Target and jammer signals are modelled as plane waves. All waves have the same wavelength λ_0, and the antenna elements are spaced $\lambda_0/2$ apart. Each wave has a random phase drawn from a uniform distribution on $[0, 2\pi]$.

The output, V_i, from antenna element i is a complex voltage, consisting of the (true or false) target signal s_i, the NLI jammer signals b_i, thermal noise n_i, and a calibration error $\varepsilon_i^{\text{cal}}$.

$$V_i = (s_i + b_i + n_i)\left(1 + \varepsilon_i^{\text{cal}}\right)$$

Both the thermal noise and the calibration error are modelled as zero-mean, complex, gaussian noise, uncorrelated between antenna elements. The thermal noise has a standard deviation $\sigma_{\text{th}} = 1$ and the calibration error has a standard deviation $\sigma_{\text{cal}} = 0.02$. The calibration error is added in order to avoid unrealistically low sidelobe levels.

The antenna array will always be steered at boresight, so the main channel output (before SLC) is

$$V_{\text{in}} = \sum_{i=1}^{N} w_i^{\text{tap}} V_i,$$

where w_i^{tap} is the tapering weight of antenna element i.

2.2.1.1 Signal-to-noise ratio

In this report, signal-to-noise-ratio (SNR) and jammer-to-noise-ratio (JNR) refer to the ratio for one antenna element. They are defined as

$$\text{SNR} = 10 \log_{10} \left(\frac{a_t^2}{\sigma_{\text{th}}^2} \right) \text{ dB}$$

$$\text{JNR} = 10 \log_{10} \left(\frac{a_j^2}{\sigma_{\text{th}}^2} \right) \text{ dB},$$

where a_t and a_j are the amplitudes of the target and jammer respectively and σ_{th}^2 is the variance of the thermal noise in that antenna element. Note that SNR in the main channel, SNR_{sum}, differs from SNR for one antenna element. SNR_{sum} is highly dependent on target direction relative to mainlobe direction. If the antenna is steered at boresight, SNR_{sum} is given by

$$\text{SNR}_{\text{sum}} = 10 \log_{10} \left(\frac{a_t^2}{\sigma_{\text{th}}^2} \frac{\left| \sum_{i=1}^{N} w_i e^{j\pi u_t i} \right|^2}{\sum_{i=1}^{N} |w_i|^2} \right) \text{ dB},$$

where w_i is the weights of the antenna elements in the main channel.

2.2.2 The covariance matrix

As described in Section 1.2.2, a fundamental part of SLC is knowledge of the covariance of the unwanted part (i.e. inteference and noise) of the signals received by the auxiliary antennas. Due to its importance in radar signal processing, the task of estimating the covariance matrix has been thoroughly studied. However, covariance estimation is outside the scope of this thesis, and analytical expressions for the covariance matrix for the model problem are therefore derived in this section. In order to study the effect of non-perfect estimations, a simple model for covariance matrix estimation error is also introduced.

Let $\mathbf{q} = [q_1 \ldots q_M]^{\text{T}}$ be the signals of jammers and thermal noise received by the M auxiliary antennas. Suppose there are J NLI-jammers. The i:th element in $\mathbf{q}$ is then given by

$$q_i = \sum_{k=1}^{J} a_k e^{j(\varphi_i(u_k) + \xi_k)} + n_i, \tag{2.2}$$

where a_k is the amplitude and ξ_k is the random phase of the k:th jammer signal and $\varphi_i(u_k)$ is the phase shift between the antenna element in question and a reference point for a wave from direction u_k. The expression for $\varphi_i(u_k)$ is given in (1.1).

The covariance matrix $\mathbf{Q}$ is defined as:

$$\mathbf{Q} = \begin{bmatrix} \mathrm{Cov}[q_1, q_1] & \dots & \mathrm{Cov}[q_1, q_M] \\ \vdots & \ddots & \vdots \\ \mathrm{Cov}[q_M, q_1] & \dots & \mathrm{Cov}[q_M, q_M] \end{bmatrix},$$

Since the elements in $\mathbf{q}$ have zero mean (all phases are equally probable), this simplifies to

$$\mathbf{Q} = \mathrm{E}\big[\mathbf{q}\mathbf{q}^{\mathrm{H}}\big] = \begin{bmatrix} \mathrm{E}[q_1\overline{q_1}] & \dots & \mathrm{E}[q_1\overline{q_M}] \\ \vdots & \ddots & \vdots \\ \mathrm{E}[q_M\overline{q_1}] & \dots & \mathrm{E}[q_M\overline{q_M}] \end{bmatrix}.$$

Using the expression for $\mathbf{q}$ defined in (2.2) and assuming uncorrelated jammers, the elements in $\mathbf{Q}$ is given by

$$Q_{nm} = \mathrm{E}[q_n\overline{q_m}] = \sum_{k=1}^{J} a_k{}^2 e^{j\pi(d_n - d_m)u_k} + \mathrm{E}[n_n\overline{n_m}],$$

where d_i is the distance in antenna elements between a reference point and auxiliary antenna i. Further, due to the assumption that the thermal noise is zero-mean and uncorrelated between antenna elements,

$$\mathrm{E}[n_n\overline{n_m}] = \begin{cases} 0 & \text{if } n \neq m \\ \sigma_{\mathrm{th}}^2 & \text{if } n = m \end{cases}$$

Thus,

$$Q_{nm} = \begin{cases} \displaystyle\sum_{k=1}^{J} a_k{}^2 + \sigma_{\mathrm{th}}^2, & n = m \\ \displaystyle\sum_{k=1}^{J} a_k{}^2 e^{j\pi(d_m - d_n)u_k}, & n \neq m \end{cases}$$

Analogous reasoning for the cross-covariance vector $\mathbf{R}$ defined as

$$\mathbf{R} = \begin{bmatrix} \mathrm{Cov}[q_{\mathrm{in}}, q_1] \\ \dots \\ \mathrm{Cov}[q_{\mathrm{in}}, q_M] \end{bmatrix}$$

yields

$$\mathbf{R} = \sum_{k=1}^{J} \mathbf{R}_k + \mathbf{n},$$

13

where $\mathbf{R}_k$ is the covariance vector for one NLI-jammer and $\mathbf{n} = [\sigma_{\text{th}}^2, \sigma_{\text{th}}^2, \ldots, \sigma_{\text{th}}^2]^{\text{T}}$. $\mathbf{R}_k$ is given by

$$\mathbf{R}_k = \begin{bmatrix} e^{-j\pi d_{i_1} u_k} \\ e^{-j\pi d_{i_2} u_k} \\ \vdots \\ e^{-j\pi d_{i_M} u_k} \end{bmatrix} |a_k|^2 \sum_{i=1}^{N} \left(w_i e^{j\pi d_i u_k} \right),$$

where $i_1, \ldots, i_M$ are the indices of the auxiliary antennas.

2.2.2.1 Estimation error model

For modelling estimation error of the covariance matrix $\mathbf{Q}$, the following model is used

$$\hat{\mathbf{Q}} = \text{diag}(1 + \boldsymbol{\varepsilon}^{\text{est}})\mathbf{Q}\,\text{diag}(1 + \boldsymbol{\varepsilon}^{\text{est}})^{\text{H}}, \tag{2.3}$$

where $\boldsymbol{\varepsilon}^{\text{est}}$ is a vector with uncorrelated, complex disturbances drawn from a complex, gaussian distribution with zero mean and standard deviation σ_{est}. $\text{diag}(\mathbf{v})$ represents a quadratic matrix with the elements in $\mathbf{v}$ as its diagonal elements and with all other elements 0. The model is chosen because it is simple and preserves the hermitian property of $\mathbf{Q}$. Analogous reasoning for the cross-covariance vector $\mathbf{R}$ yields

$$\hat{\mathbf{R}} = (1 + \varepsilon^{\text{est}})\mathbf{R}\,\text{diag}(1 + \boldsymbol{\varepsilon}^{\text{est}})^{\text{H}},$$

where ε^{est} is a scalar drawn from the same distribution.

2.2.3 Simulation method

In order to determine P_d and P_{fa}, the mainlobe and sidelobe region must first be defined. Since the antenna pattern is continuous, it is not obvious where to draw the line and multiple definitions exists. We have chosen to define the mainlobe region as the *half power beam width* of the undisturbed antenna pattern, while the sidelobe regions are defined as the region outside the first nulls. This results in a undefined region between the half power beam width and the first null, which is not considered. With those definitions and the tapering used, the mainlobe region is defined as

$$|u| \leq 0.0125,$$

corresponding to a width of 1.4°, and the sidelobe region is defined as

$$|u| \geq 0.0367,$$

corresponding to a gap of 4.2°.

P_d and P_{fa} are computed using Monte Carlo-simulations. In each simulation SNR_{sum}, JNR, σ_{est}, J and the placement of auxiliary antennas are held constant. For each data point, u_j and u_t are drawn from uniform distributions on the sidelobe/mainlobe regions. The amplitude of the target signal is then adjusted to get the desired SNR_{sum} in the main channel. Each simulation uses 5000 data points with u_t in mainlobe and 10 000 data points with u_t in sidelobe region.

We noted a tendency for the sidelobe level in the main channel to increase dramatically when covariance estimation errors are introduced for $M > J$. In order to avoid this, only the J first auxiliary antennas are used for SLC in the main channel. In a situation where the number of jammers is not known beforehand, this could for instance be accomplished by Vandermonde decomposition of the covariance matrix in order to determine J, or simply by computing V_m using different number of auxiliary antennas and choose the smallest value. The latter method should work because the best weights are those that cancel out most of the jammer effect, hence would result in the lowest V_m. When SLC is applied to the guard channel, all auxiliary antennas are used.

3
Results

In this chapter, the results of the simulations are presented. The performance is presented with ROC-curves, which are plots of $P_d(T)$ versus $P_{fa}(T)$, parameterized with T. For illustration purposes, plots with Youden's index, Y, are also presented. Youden's index is defined as

$$Y(T) = P_d(T) - P_{fa}(T).$$

It is a measure that ranges from -1 to 1, where $Y = 1$ means a perfect performance, i.e. all false targets and no true targets are blanked. Youden's index is a measure that puts equal importance on maximizing P_d and minimizing P_{fa}. It is used in this report mainly because it is easy, but in real applications maximizing P_d or minimizing P_{fa} might be valued higher than the other.

Unless stated otherwise, the simulations are run using the following parameters: $\text{SNR}_{\text{sum}} = 10\,\text{dB}$, $\text{JNR} = 40\,\text{dB}$, $\sigma_{\text{est}} = 0.1$ and 1 NLI-jammer.

3.1 The undisturbed case

When no NLI-jammers are present, all three tested algorithms reduce to ordinary SLB. For comparison, the performance of SLB when no NLI-jammers are present is shown in Figure 3.1. As seen in Figure 3.1b, it is possible to choose a blanking threshold T so that all false targets and no true targets are blanked. Figure 3.1b also shows that SNR_{sum} influences P_d but not P_{fa}.

3.2 Effect of auxiliary antenna position

In order to investigate how the placement of the auxiliary antennas influence the performance of the guard functions, three different placements are tested. The positions are presented in Table 3.1. Examples of the resulting antenna patterns for guard and main channel are shown in Figure 3.2 and ROC-curves are shown

Table 3.1: Auxiliary antenna placements used.

	guard	aux
Placement 1	1	2, 3, 4
Placement 2	1	2, 3, 100
Placement 3	1	8, 37, 100

(a) ROC-curve

(b) Youdens index

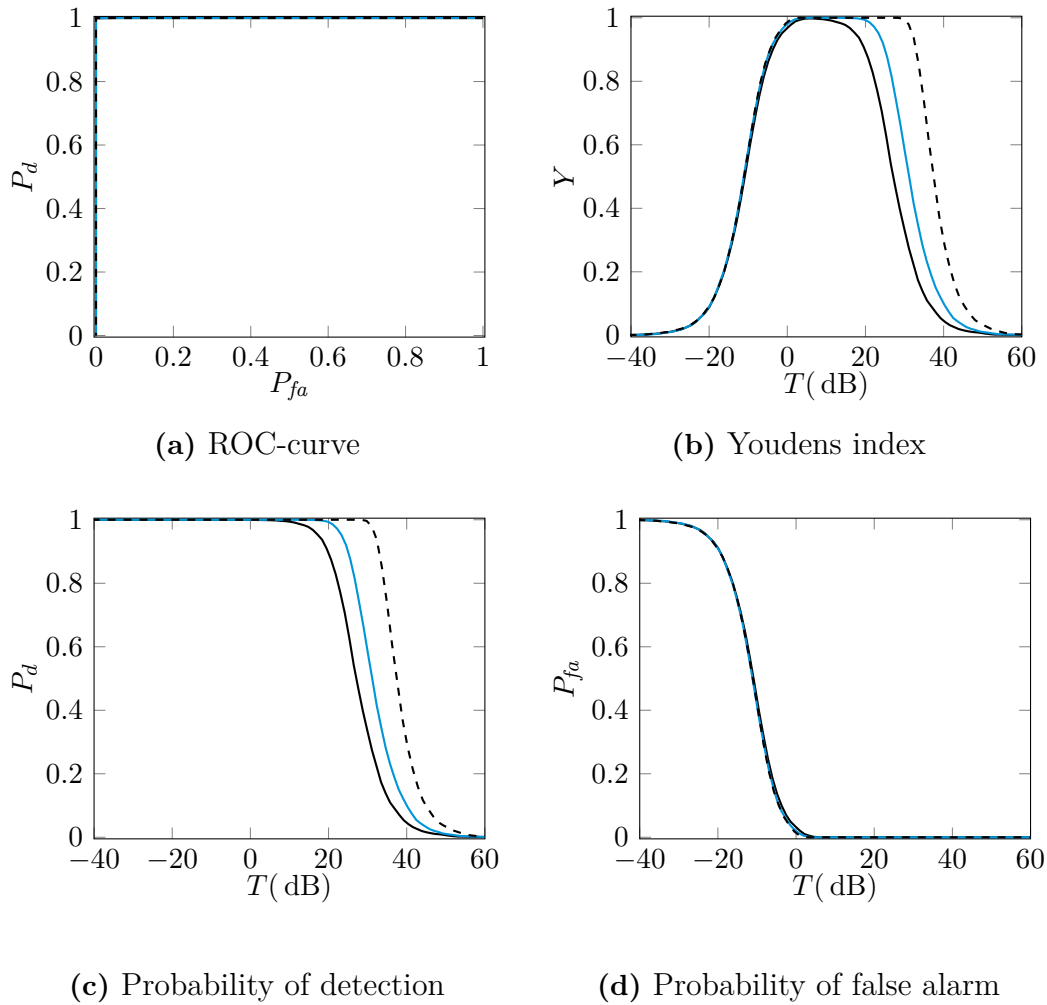**(c)** Probability of detection

(d) Probability of false alarm

Figure 3.1: The performance of SLB when no NLI-jammers are present. $\text{SNR}_{\text{sum}} = 5\,\text{dB}$ (black), $\text{SNR}_{\text{sum}} = 10\,\text{dB}$ (blue) and $\text{SNR}_{\text{sum}} = 20\,\text{dB}$ (dashed).

(a) SLCg Placement 1

(b) SLCg max Placement 1

(c) SLCg Placement 2

(d) SLCg max Placement 2
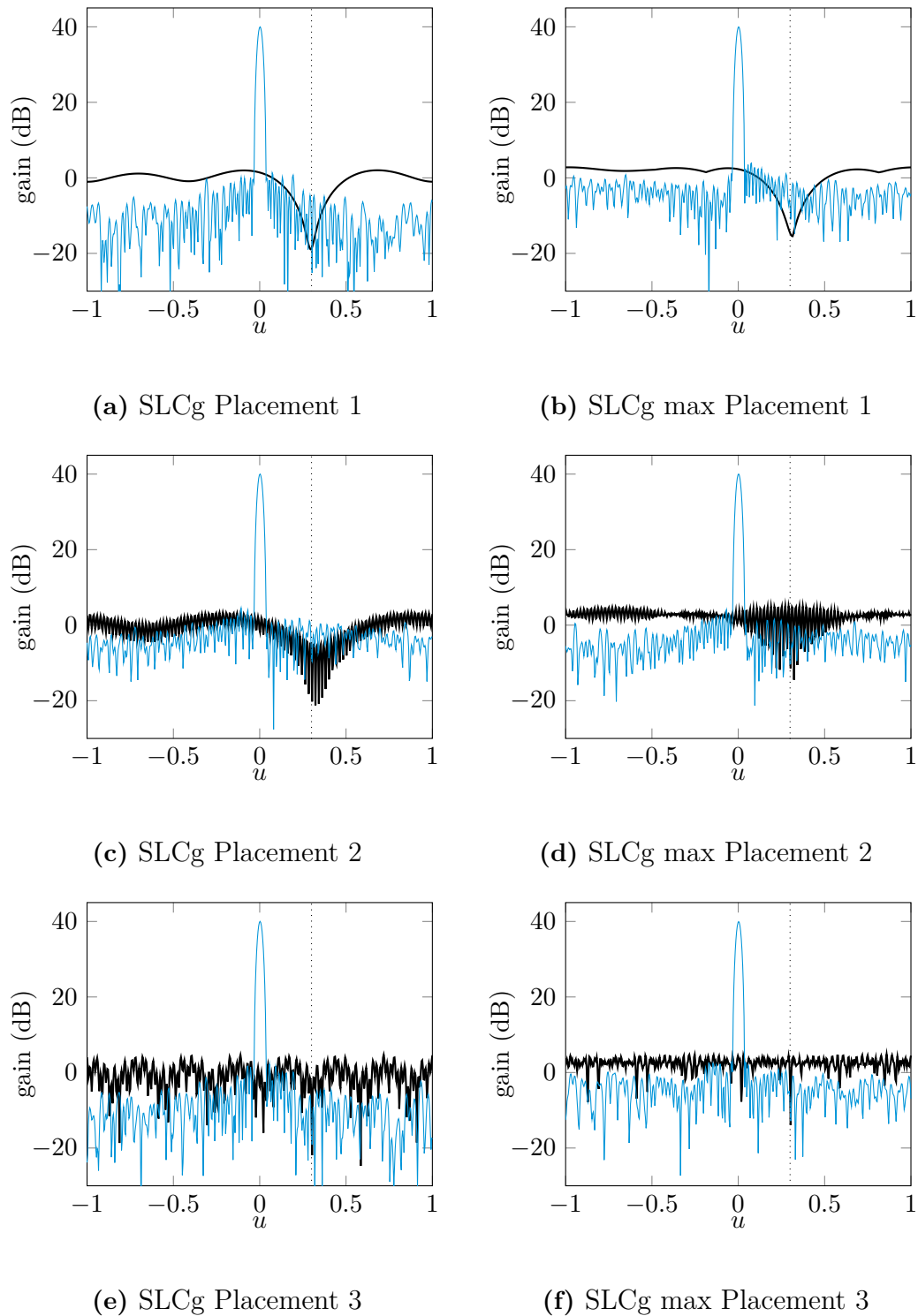
(e) SLCg Placement 3

(f) SLCg max Placement 3

Figure 3.2: Illustration of the effect of auxiliary antenna position on main channel pattern (blue) and guard channel pattern (black) for $u_j = 0.3$. The positions are defined in Table 3.1.
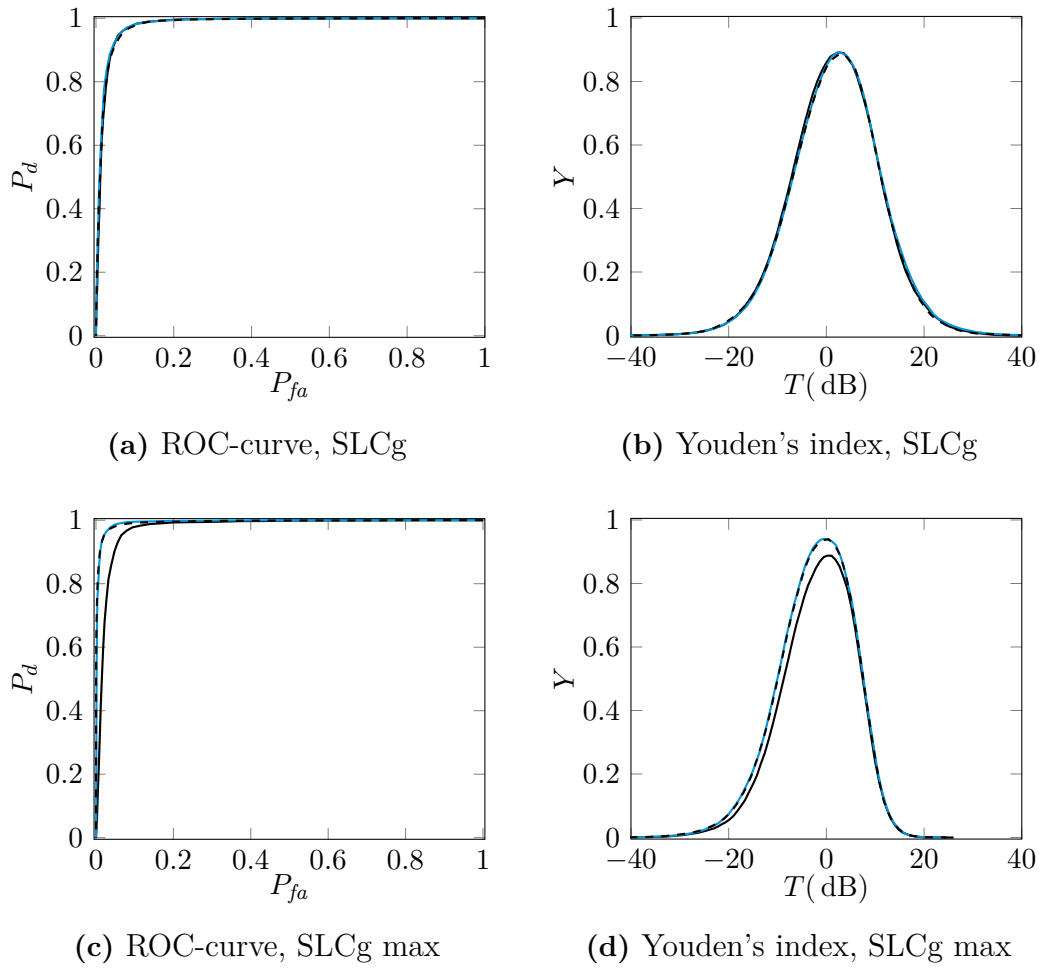
(a) ROC-curve, SLCg

(b) Youden's index, SLCg

(c) ROC-curve, SLCg max

(d) Youden's index, SLCg max

Figure 3.3: ROC-curves and Youden's index (J) for Placement 1 (black), Placement 2 (blue) and Placement 3 (dashed).

(a) ROC-curve

(b) Youden's index

(c) Probability of detection

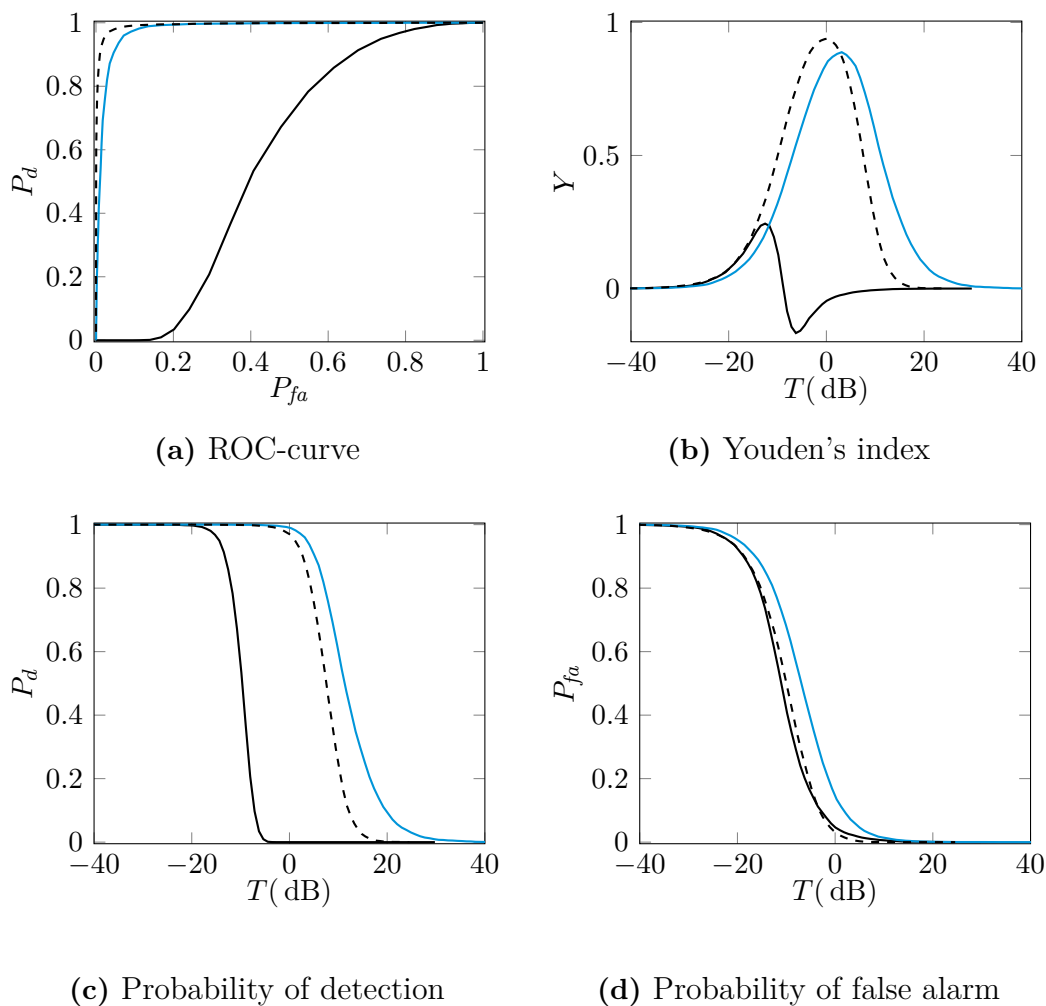**(d)** Probability of false alarm

Figure 3.4: Comparison of the three tested guard functions No SLCg (black), SLCg (blue) and SLCg max (dashed).

in Figure 3.3. Although the placement clearly influences the shape of the guard antenna diagram, the effect on overall performance is small. In fact, as seen in Figure 3.3a placement has no significant effect on performance of SLCg. For SLCg max, Placement 1 leads to a minor decrease in performance, while no significant difference between Placement 2 and Placement 3 is observed. This is shown in Figure 3.3c. For the rest of the simulations, Placement 3 is used. Since the placement of auxiliary antennas does not influence the guard channel in No SLCg, it is not included here.

3.3   Comparison between methods

Figure 3.4 shows a comparison between the three tested guard functions. For those parameters, SLCg max has a bit better performance than SLCg, while No SLCg has a much worse performance and could in fact be considered useless. In the rest of this chapter the effect of SNR_{sum}, JNR, covariance estimation errors and number of jammer on SLCg and SLCg max are presented.
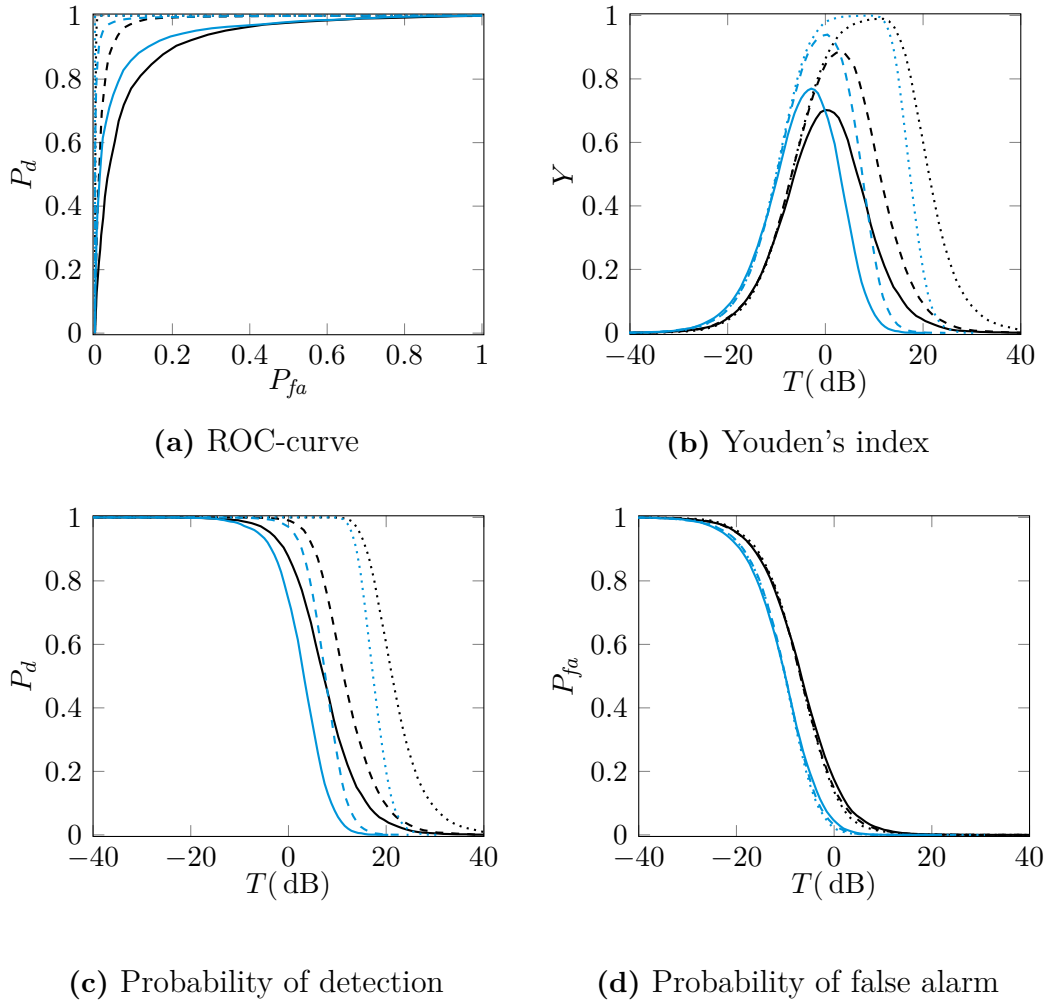
(a) ROC-curve

(b) Youden's index

(c) Probability of detection

(d) Probability of false alarm

Figure 3.5: Effect of SNR$_{\text{sum}}$ on performance of SLCg(black) and SLCg max(blue) for SNR = 5 dB (full), 10 dB (dashed) and 20 dB (dotted).

3.4 Effect of JNR and SNR$_{\text{sum}}$

The effect of SNR$_{\text{sum}}$ and JNR on performance of SLCg and SLCg max are shown in Figure 3.5 and Figure 3.6. The effects are similar, both influences P_d but not P_{fa}. An increase in SNR$_{\text{sum}}$ or a decrease in JNR increases performance.

3.5 Effect of covariance estimation error

The effect of errors in the covariance estimations used for computing SLC-weights is shown in Figure 3.7, where it is shown that estimation error influences P_d but not P_{fa}.
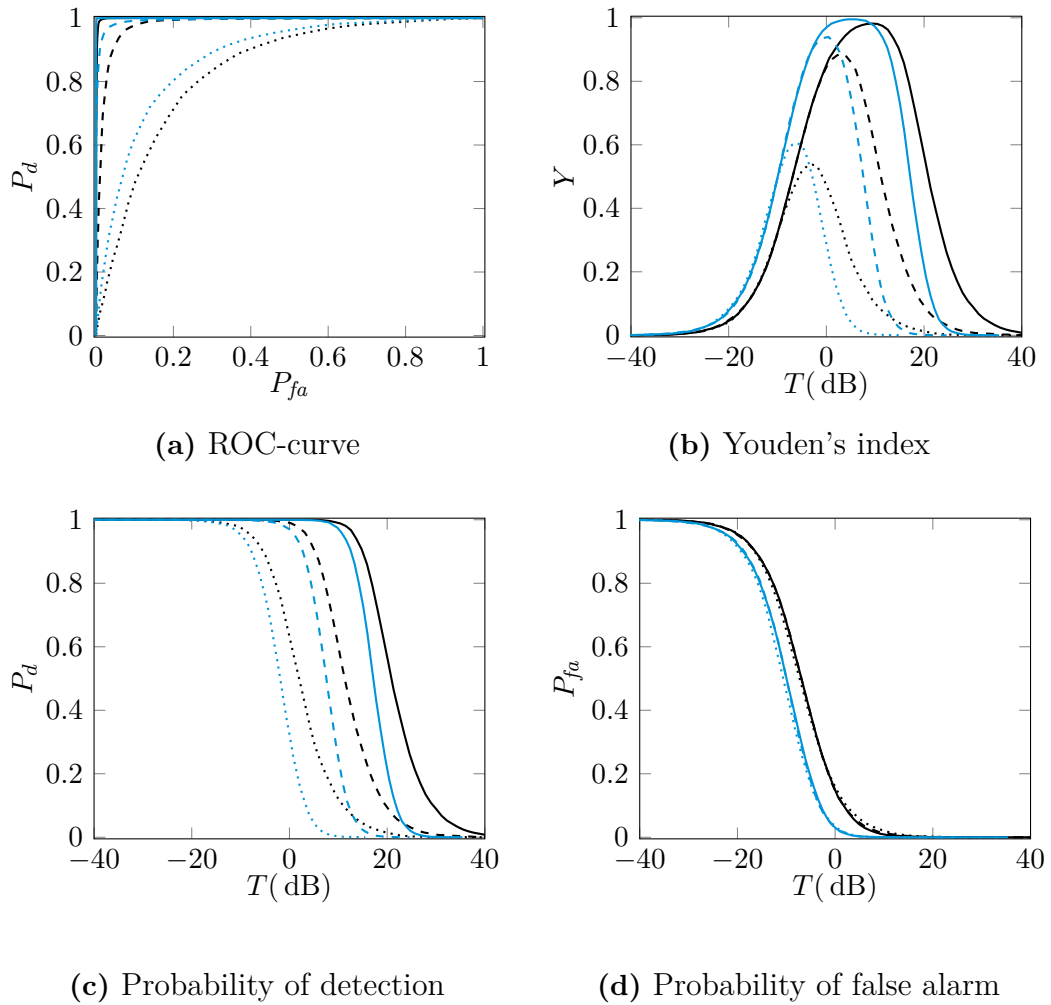
(a) ROC-curve

(b) Youden's index

(c) Probability of detection

(d) Probability of false alarm

Figure 3.6: Effect of JNR on performance of SLCg (black) and SLCg max (blue) for JNR = 30 dB (full), 40 dB (dashed) and 50 dB (dotted).

(a) ROC-curve

(b) Youden's index

(c) Probability of detection

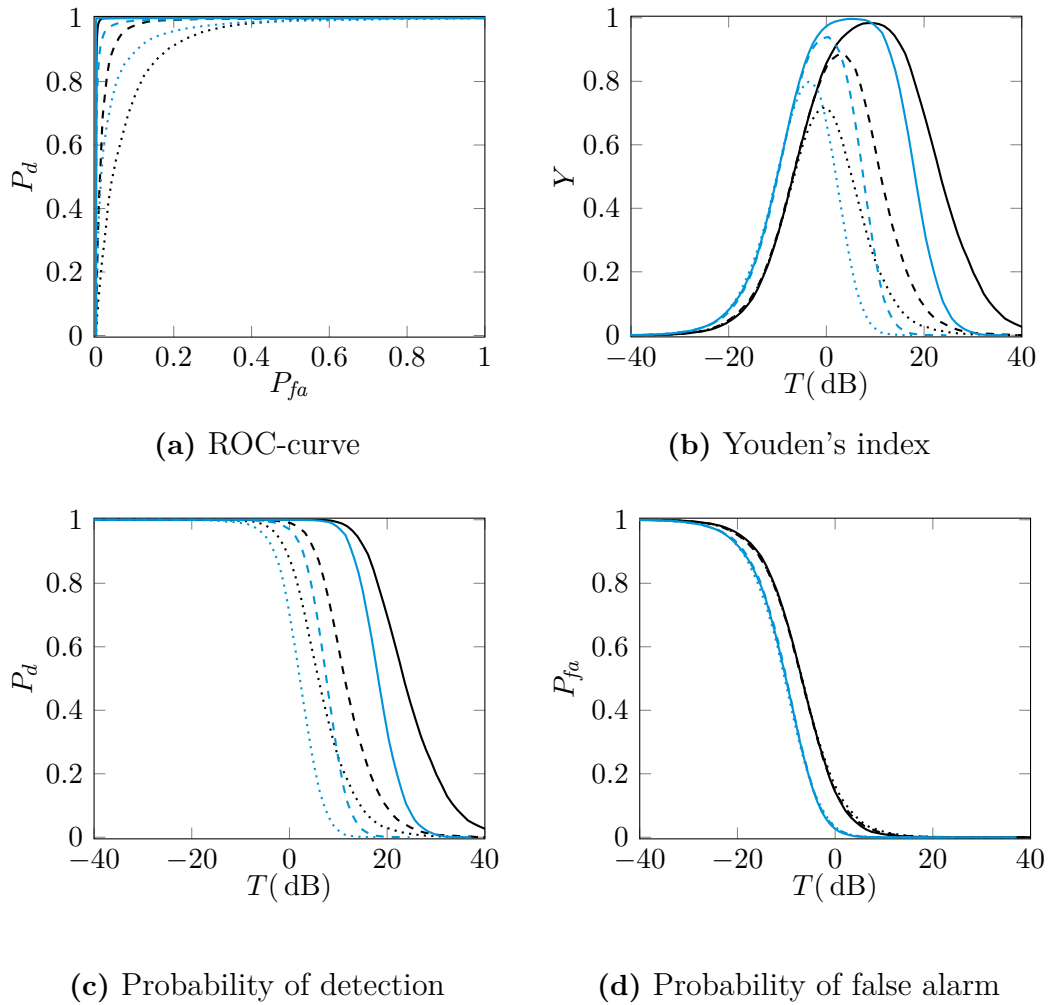**(d)** Probability of false alarm

Figure 3.7: Effect of covariance estimation error on SLCg (black) and SLCg max (blue), for no error (full), $\sigma_{\text{est}} = 0.1$ (dashed) and $\sigma_{\text{est}} = 0.2$ (dotted).
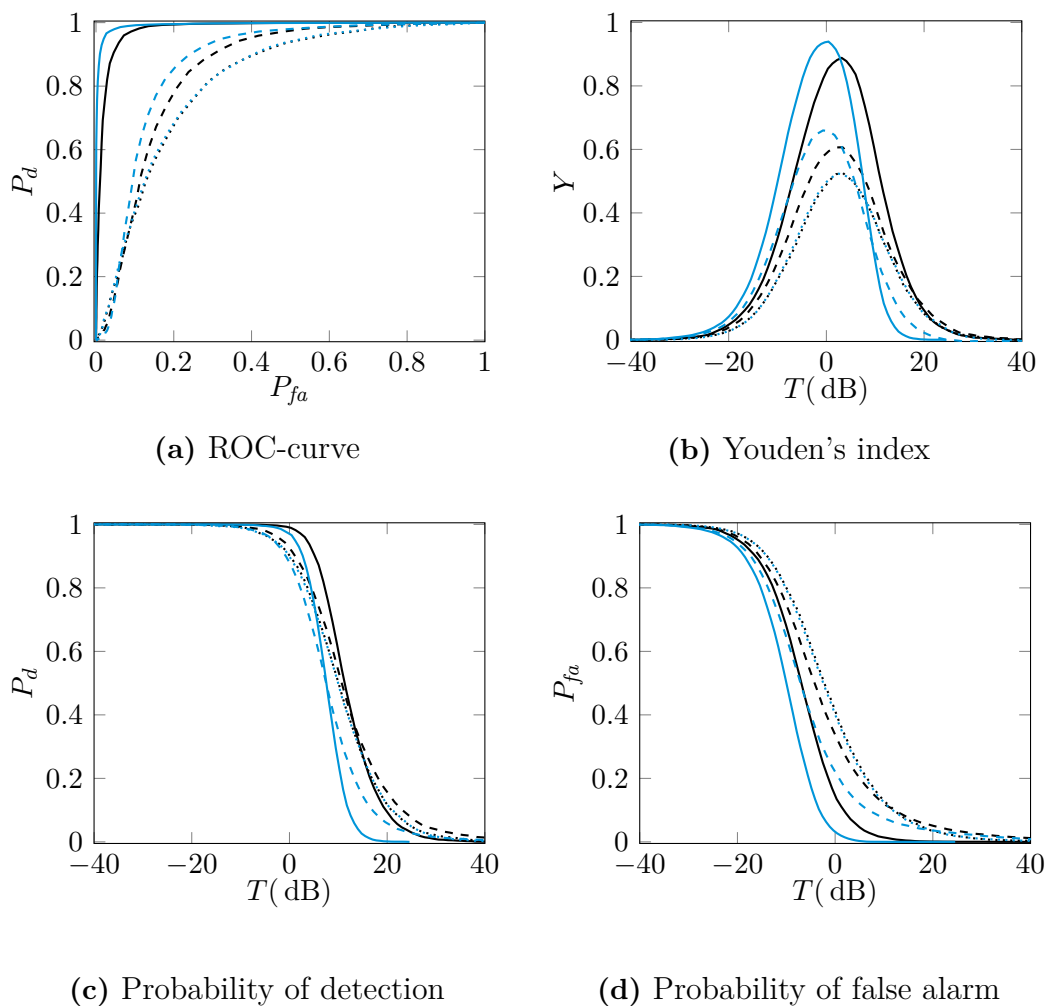
(a) ROC-curve

(b) Youden's index

(c) Probability of detection

(d) Probability of false alarm

Figure 3.8: Effect of the number of jammers on SLCg (black) and SLCg max (blue) for one jammer (full), 2 jammers (dashed) and three jammers (dotted).

3.6 More than one jammer

The performance of SLCg and SLCg max when more than one NLI-jammer are present are shown in Figure 3.8. The performance of the two methods is significantly reduced for the case of more than one jammer. As expected both methods have the same performance, when the number of jammers are equal to the number of auxiliary antennas. In order to shine some light on why the performance is reduced, the effect of number of jammers without covariance estimation errors are shown in Figure 3.9. The overall performance is better in this case, but the same tendencies of reduced performance for more than one jammer is seen. In Figure 3.10 the effect of auxiliary antenna placement is revisited, but for the case of three jammers. Since SLCg max reduces to SLCg when the number of jammers is the same as the number of auxiliary antennas, only SLCg is shown.

(a) ROC-curve

(b) Youden's index

(c) Probability of detection
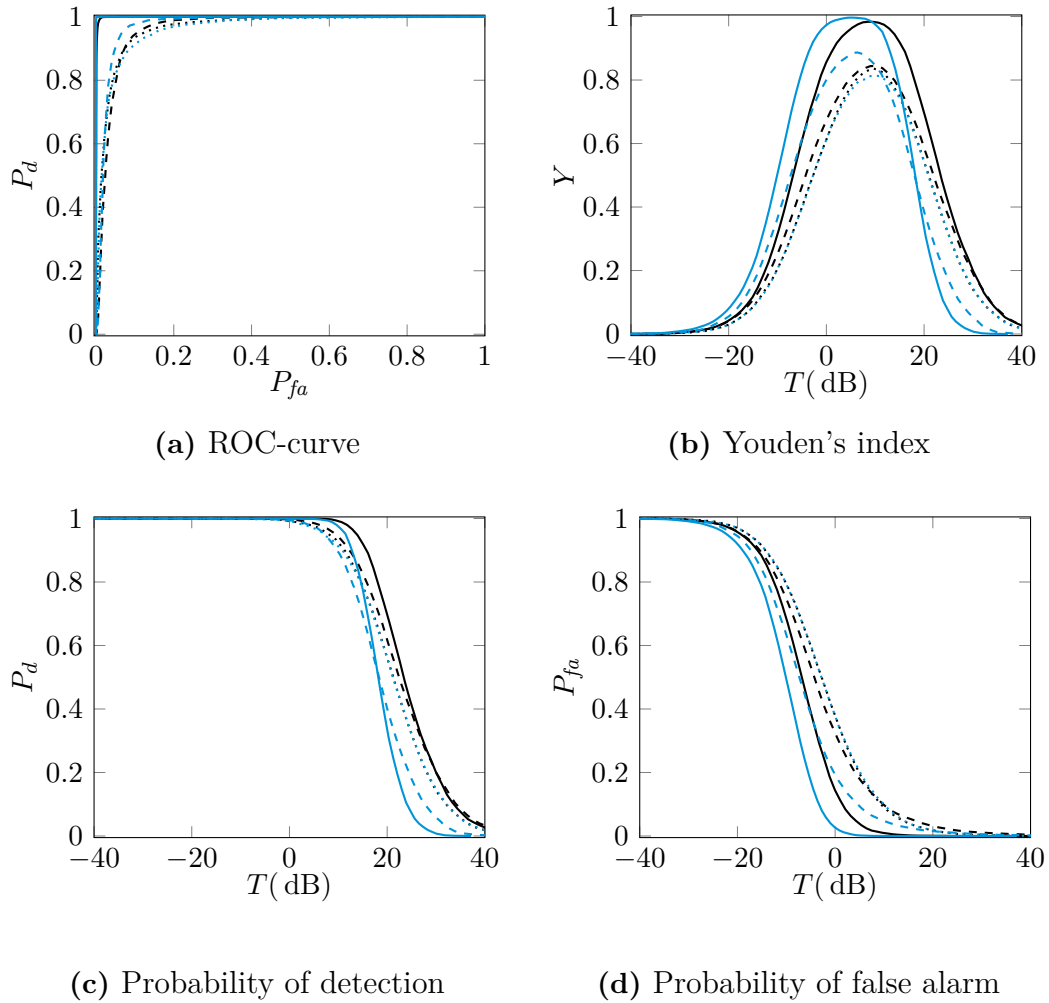
(d) Probability of false alarm

Figure 3.9: Effect on the number of jammers on SLCg (black) and SLCg max (blue) with no error in covariance estimation. Lines correspond to one jammer (full), 2 jammers (dashed) and three jammers (dotted).

(a) ROC-curve

(b) Youden's index

(c) Probability of detection

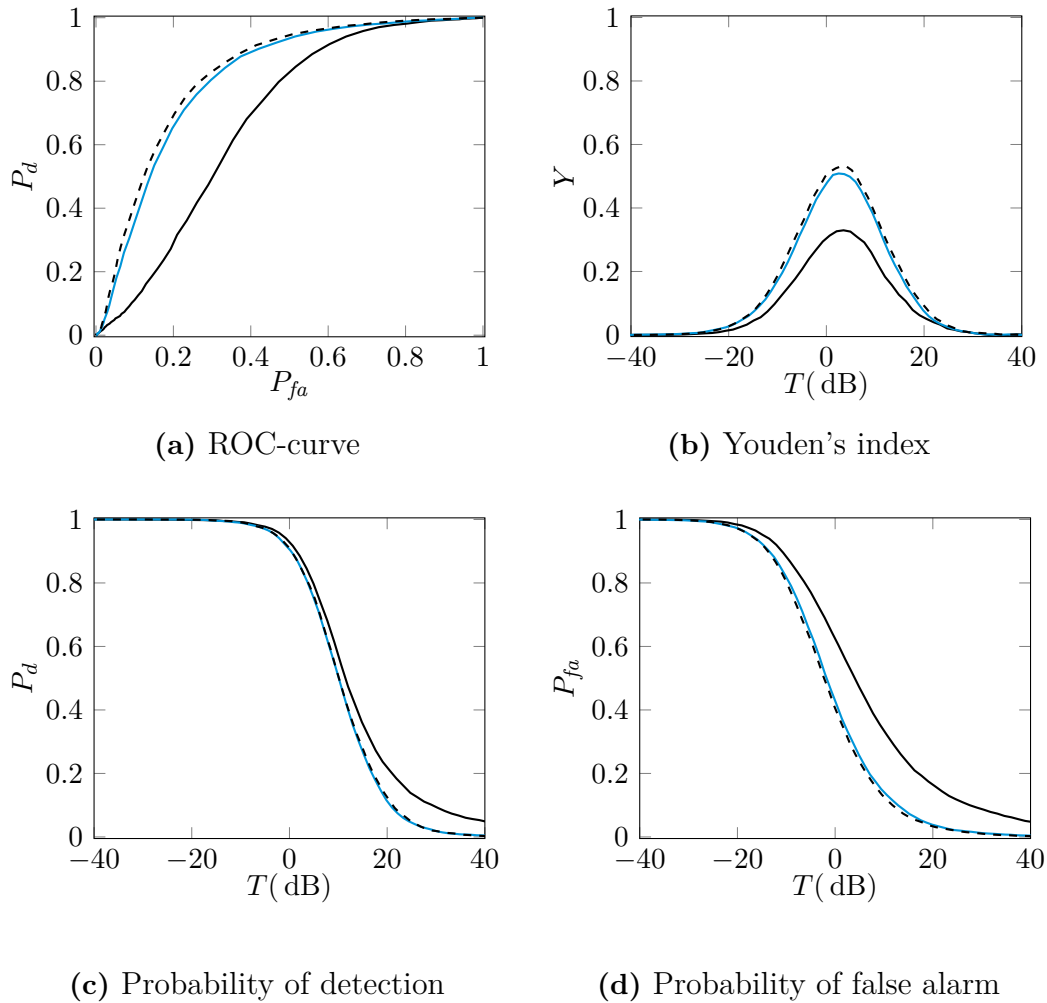**(d)** Probability of false alarm

Figure 3.10: Effect of auxiliary antenna placement on SLCg when three NLI-jammers are present. Lines corresponds to Placement 1 (black), Placement 2 (blue) and Placement 3 (dashed).

4
Discussion

Regarding the placement of guard and auxiliary antennas, it seems beneficial to cover a large span by using antenna elements in both edges of the antenna array, as illustrated in Figure 3.3 and Figure 3.10. We believe this is because a large span between the antennas creates a high frequency component in the guard channel. Otherwise the placements does not seem to affect the performance much regarding the guard channel. But as shown, errors in the covariance estimation highly affect performance. Thus it is probably more important to choose auxiliary antenna placement for optimising covariance estimation than avoiding deep notches in non-jammer directions of the guard channel.

Increasing JNR, decreasing SNR and increasing covariance estimation errors all have similar effects, namely to decrease P_d without affecting P_{fa}. This can be interpreted as covariance estimation errors decrease the quality of nulls, making them more shallow so that more jammer energy leaks in. Since the effect of NLI-jammers is an increase in noise level, it is expected that increasing JNR and decreasing SNR has similar results.

As seen in Figure 3.8, the number of NLI-jammers greatly affects performance. One possible explanation for this could be that the nulls in the guard channel in jammer directions are too shallow, so that more jammer energy leaks in simply because there are more jammers. This explanation does not seem to be the main reason for two reasons. Firstly, the effect is large also when no covariance estimation errors are added. Secondly, the behaviour of P_d and P_{fa} differs significantly from the case of increasing JNR. Another possibility is that multiple nulls make restrictions on the guard channel antenna pattern, which if the nulls are close enough can force down the antenna pattern in the region between nulls. Comparison between Figure 3.3 and Figure 3.10 confirms this hypothesis, since auxiliary placement influences the result in SLCg for 3 jammers, but not for 1 jammer.

It is worth noticing that if one of the computed guard channels produced in SLCg max fails at introducing a null in the antenna pattern in the desired direction, this guard channel will have the highest amplitude (due to jammer energy leaking in), and will thus be the used guard channel. In the worst case, this will produce a similar result as No SLCg, and thus have a very bad performance. Failure to produce a null in the desired direction can for example happen for a unlucky combination of jammer directions and auxiliary antenna placement, as derived in Section 1.2.2.1. The same failure could of course happen in SLCg as well, but the probability of this happening in SLCg max is higher. This effect has not been observed in this project, but might pose a problem in scenarios where the risk of failing to introduce a null is high.

4.1 Different approaches

The guard functions evaluated in this report all take the approach of using some kind of guard channel to determine whether the detection is in the mainlobe or sidelobe. Another approach to the problem would be to estimate the the direction of the target signal directly from the auxiliary antenna signals. This problem is analogous to that of frequency estimation. If the antenna elements used are few and far (i.e. more than half a wavelength) apart, the problem is sparse or undersampled. See for example [15] for an extensive review of method for solving such problems. For the problem treated in this report however, two major problems arises: (i) few samples and (ii) low (possibly negative) SNR in auxiliary antennas when the target is located in the mainlobe. There are few samples because there are few auxiliary antennas and target signal is typically short, so multiple snapshots of the same target will in general not be available. The problem of sparse direction-of-arrival estimations for the combinations low SNR with many snapshots and few snapshots with high SNR is treated in [16], but not the combination of low SNR and few snapshots.

5

Conclusion

In conclusion, both SLCg and SLCg max work well in the case of one jammer, and are definitely a much better alternative than to use the guard channel directly when NLI is present. In the scenarios investigated here, SLCg max in general performs better than SLCg, but as discussed in the previous section this might not always be the case. Additional antennas should be placed on both edges of the antenna array, but otherwise the placement of auxiliary antennas does not effect the performance of the guard functions substantially. However, the placement can affect the performance indirectly, by influencing SLC in general and covariance estimation errors. The performance of SLCg and SLCg max is reduced drastically when more than one NLI source are present.

5.1   Future work

In this project, the guard functions are evaluated using a highly simplified model. The next step should be to investigate the effect of allowing target and jammers to have a frequency range instead of a single frequency, to use more realistic antenna models and to study the effect of clutter and correlated interference, such as multipath echoes. This could either be done by using more complex models, or, ideally, by evaluating the guard functions on real radar data. Influence of polarisation, especially when jammers and target have different polarisation, may also be of interest.

As shown in Section 1.2.2.1, the SLC weights can in general be chosen in infinitely many ways, when the number of NLI-jammers are fewer than the number of auxiliary antennas. It may be worth investigating if there is a better way to choose the weights than using (1.3) in order to accomplish a desirable guard channel pattern.

5. Conclusion

Bibliography

[1] J. Agar, "Science and the second world war", in *Science in the Twentieth Century and Beyond*, Polity, 2013, pp. 268–275.

[2] S. Sinha, C. Jeganathan, and L. Sharma, "A review of radar remote sensing for biomass estimation", *International Journal of Environmental Science and Technology*, vol. 12, no. 5, pp. 1779–1792, May 2015.

[3] M. Klemm, I. J. Craddock, J. A. Leendertz, A. Preece, and R. Benjamin, "Radar-based breast cancer detection using a hemispherical antenna array –experimental results", *IEEE Transactions on Antennas and Propagation*, vol. 57, no. 6, pp. 1692–1704, Jun. 2009.

[4] M. Skolnik, "An introduction and overview of radar", in *Radar Handbook*, M. Skolnik, Ed., 3rd ed., New York: McGraw-Hill, 2008.

[5] J. Frank and J. D. Richards, "Phased array radar antennas", in *Radar Handbook*, M. Skolnik, Ed., 3rd ed., New York: McGraw-Hill, 2008.

[6] W. G. Carrara, R. S. Goodman, and R. M. Majewski, "Sidelobe control in SAR imagery", in *Spotlight Synthetic Aperture Radar -Signal Processing Algorithms*, Boston: Artech House, 1995, pp. 507–529.

[7] F. Bandiera and A. Farina, "Detection algorithms to discriminate between radar targets and ECM signals", *IEEE Trans. on Signal Process.*, vol. 59, no. 12, pp. 5984–5993, Dec. 2010.

[8] A. Farina, "Antenna-related ECCM", in *Radar Handbook*, M. Skolnik, Ed., 3rd ed., New York: McGraw-Hill, 2008.

[9] D. Orlando, "A novel noise jamming detection algorithm for radar applications", *IEEE Signal Process. Lett*, vol. 24, no. 2, pp. 206–210, Feb. 2017.

[10] J. Kocz, F. H. Briggs, and J. Reynolds, "Radio frequency interference removal through the application of spatial filtering techniques on the parkes multibeam receiver", *The Astronomical Journal*, vol. 140, no. 6, pp. 2086–2094, 2010.

[11] U. Nickel, "Design of generalised 2d adaptive sidelobe blanking detectors using the detection margin", *Signal Processing*, vol. 90, no. 5, pp. 1357–1372, 2010.

[12] D. A. Shnidman and N. R. Shnidman, "Sidelobe blanking with expanded models", *IEEE Transactions on Aerospace and Electronic Systems*, vol. 47, no. 2, pp. 790–805, Apr. 2011.

[13] A. Farina, "Sidelobe canceller (SLC) system", in *Antenna-Based Signal Processing Techniques for Radar Systems*, Boston: Artech House, 1992, pp. 95–103.

[14] A. Farina, L. Timmoneri, and R. Tosini, "Cascading SLB and SLC devices", *Signal Process.*, vol. 45, no. 2, pp. 261–266, Aug. 1995.

[15]   Z. Yang, J. Li, P. Stoica, and L. Xie, "Sparse methods for direction-of-arrival estimation", *CoRR*, vol. abs/1609.09596, 2017. arXiv: `1609.09596v2`. [Online]. Available: `http://arxiv.org/abs/1609.09596v2`.

[16]   A. Nehorai, D. Starer, and P. Stoica, "Direction-of-arrival estimation in applications with multipath and few snapshots", *Circuits, Systems and Signal Processing*, vol. 10, no. 3, pp. 327–342, Sep. 1991.